BULLETIN OF THE POLISH ACADEMY OF SCIENCES
TECHNICAL SCIENCES, Vol. 59, No. 2, 2011
DOI: 10.2478/v10175-011-0027-9

Numerical solutions of magnetohydrodynamic equations

K. MURAWSKI*

Faculty of Mathematics, Physics and Informatics, UMCS, 10 Radziszewskiego St., 20-031 Lublin, Poland

Abstract. In this paper we review several mathematical aspects in numerical methods for magnetohydrodynamic equations. The intrinsic complexity and the requirements of the selenoidity condition make numerical solutions of these equations a formidable task. We present results of advanced numerical simulations for a complex system, which reveal that the numerical methods cope very well with this task.

Key words: numerical methods for hyperbolic equations, finite volume methods, Godunov-type methods, magnetohydrodynamics.

1. Introduction

The magnetohydrodynamic (MHD) theory is the simplest self-consistent model describing the macroscopic behavior of the plasma. Despite of that the full nonlinear equations are so complex that usually significant simplifications are necessary to yield analytically tractable problems. As a result, the MHD equations usually require numerical treatment. Finite-volume methods [1] are one of several different techniques available to solve the MHD equations. They are simple to implement, easily adaptable to complex geometries, and well suited to handle nonlinear terms. Like solutions of nonlinear equations, perturbations described by the MHD equations may result in large gradients which are difficult for numerical modeling. The use of standard numerical schemes of second-order accuracy or higher (e.g., the Lax-Wendroff method) generates spurious oscillations which destroy monotonicity of the solution [2]. Lower-order schemes [3] are generally free of oscillations, but they are too dissipative [1]. Therefore, a development of more advanced schemes, which could adequately represent the large gradient profiles, was required.

Due to the intrinsic complexity of the MHD equations, the development of numerical techniques to solve these equations was slower than for hydrodynamics (HD). For a long time most numerical schemes were based on methods dependent on artificial viscosity to represent adequately shocks [4]. Although these schemes were successfully applied in the past [5], recent experience with fully conservative, high-order upwind hydrodynamic codes found latter to be superior in many applications [6]. It is therefore natural to extend such schemes to solve the MHD equations. However, converting a HD code to a MHD code is a difficult task. The difficulty results from the fact that the MHD equations possess new families of waves such as switch-on fast shocks, switch-off fast rarefactions, switch-off slow shocks, and switch-on slow rarefactions [7, 8]. It is also possible to obtain compound waves of either fast or slow waves. This exerts a considerable impact on a performance of the algorithms which are required to provide accurate capture of the entire range of such structures [9]. The other difficulty is that the MHD equations contain the magnetic field which has to satisfy the divergence-free constraint. A local nonzero divergence of magnetic field indicates the existence of magnetic monopoles within the numerical cell, which leads to non-conservation of the magnetic flux across its surface. Accumulation of the numerical errors associated with evolving the magnetic field components can lead to violation of this constraint, causing an artificial force parallel to the magnetic field, and eventually can force termination of the simulations.

Despite of the above reported problems many numerical schemes were developed for the MHD equations. These schemes reveal either conservative or non-conservative properties of the equations. The aim of this paper is to review some recently devised numerical methods for solving the MHD equations, which are illustrated in Sec. 2. Some problems present in numerical schemes for the MHD equations are discussed in Sec. 3. Results of numerical simulations of impulsively generated waves in a strongly stratified atmosphere are presented in Sec. 4. This paper is completed by summary of the main results.

2. MHD equations

The MHD equations can be written in the following form:

$$\frac{\partial \varrho}{\partial t} + \nabla \cdot (\varrho \mathbf{V}) = 0, \tag{1}$$

$$\varrho \frac{\partial \mathbf{V}}{\partial t} + \varrho \left(\mathbf{V} \cdot \nabla\right) \mathbf{V} = -\nabla p + \frac{1}{\mu} (\nabla \times \mathbf{B}) \times \mathbf{B} + \varrho \mathbf{g}, \tag{2}$$

$$\frac{\partial \mathbf{B}}{\partial t} = \nabla \times (\mathbf{V} \times \mathbf{B}), \tag{3}$$

$$\nabla \cdot \mathbf{B} = 0, \tag{4}$$

$$\frac{\partial p}{\partial t} + \nabla \cdot (p\mathbf{V}) = (1-\gamma) p \nabla \cdot \mathbf{V}, \tag{5}$$

$$p = \frac{k_{\mathrm{B}}}{m} \varrho T. \tag{6}$$

Here ϱ is mass density, $\mathbf{V}$ is flow velocity, $\mathbf{B}$ is the magnetic field, p is gas pressure, $\gamma = 5/3$ is the adiabatic index, $\mathbf{g}$ is gravitational acceleration, T is temperature, m is mean particle mass and k_{B} is the Boltzmann's constant.

*e-mail: kmur@kft.umcs.lublin.pl

It is noteworthy that the set of Eqs. (1)–(6) consists of 10 scalar equations which contain 8 unknowns. Equation (4) is the selenoidal condition which constraints the system by imposing the absence of magnetic monopoles. Equation (6) is the ideal gas law which relates ϱ, p and T. Therefore having known two quantities we can determine from this law third one as, for instance, $T = T(\varrho, p)$.

2.1. Conservative form of the MHD equations. The MHD Eqs. (1)–(5) can be written in the conservative form

$$\mathbf{q}_{,t} + \nabla \cdot \mathbf{F} = 0 \tag{7}$$

with the selenoidal condition

$$\nabla \cdot \mathbf{B} = 0. \tag{8}$$

Here the state vector

$$\mathbf{q} = (\varrho, \varrho\mathbf{v}, \mathbf{B}, E)^T \tag{9}$$

and in the gravity-free case, $\mathbf{g} = \mathbf{0}$, the flux

$$\mathbf{F} = \left(\varrho\mathbf{v}, \varrho\mathbf{v}\mathbf{v} + \mathbf{I}\left(p + \frac{B^2}{2}\right) - \mathbf{B}\mathbf{B}, \mathbf{v}\mathbf{B} - \mathbf{B}\mathbf{v}, \left(E + p + \frac{B^2}{2}\right)\mathbf{v} - \mathbf{B}(\mathbf{v}\cdot\mathbf{B})\right)^T, \tag{10}$$

where

$$E = \frac{p}{\gamma - 1} + \varrho\frac{v^2}{2} + \frac{B^2}{2} \tag{11}$$

is the total energy density, $\mathbf{I}$ is the 3×3 identity matrix, $\mathbf{v}\mathbf{v}$ stands for the 3×3 tensor $v_i v_j$, and without loosing any generality $\mathbf{B}$ is replaced by $\mathbf{B}\sqrt{\mu}$.

The momentum equation of (7) can be rewritten as

$$(\varrho\mathbf{v})_{,t} + \nabla\cdot(\varrho\mathbf{v}\mathbf{v}) + \nabla\left(p + \frac{B^2}{2}\right) - (\mathbf{B}\cdot\nabla)\mathbf{B} = \mathbf{B}(\nabla\cdot\mathbf{B}). \tag{12}$$

Clearly the term on the right hand side of this equation should be equal to zero. Any $\nabla\cdot\mathbf{B} \neq 0$ results in an unphysical force that is parallel to $\mathbf{B}$ and that exerts a destabilizing effect on numerical algorithms [10]. A remedy is to add the term $-\mathbf{B}(\nabla\cdot\mathbf{B})$ to the right hand side of Eq. (12) [10] which leads to a non-conservative form of the MHD equations.

In the finite volume method the state of Eq. (9) is advanced in time by evaluating the fluxes of Eq. (10) at the interfaces between neighboring numerical cells. These fluxes must contain some dissipation which is introduced into the system by a flux limiter which minimizes oscillations [1, 2, 11]. To eliminate these oscillations, a spatially averaged primitive state,

$$\widetilde{\mathbf{q}} = (\overline{\varrho}, \overline{\mathbf{v}}, \overline{\mathbf{B}}, \overline{E})^T \tag{13}$$

may be required at the interfaces [12–15].

2.2. Non-conservative equations. The MHD equations can be rewritten in the non-conservative form (e.g., [16])

$$\mathbf{q}_{,t} + \nabla\cdot\mathbf{F} = -\nabla\cdot\mathbf{B}(0, \mathbf{B}, \mathbf{v}, \mathbf{v}\cdot\mathbf{B})^T, \quad \nabla\cdot\mathbf{B} = 0. \tag{14}$$

The induction equation can now be expressed as

$$\mathbf{B}_{,t} + \mathbf{v}(\nabla\cdot\mathbf{B}) + \mathbf{B}(\nabla\cdot\mathbf{v}) - (\mathbf{B}\cdot\nabla)\mathbf{v} = 0. \tag{15}$$

Hence by taking the divergence of both sides and using mass continuity equation, we get

$$\left(\frac{\nabla\cdot\mathbf{B}}{\varrho}\right)_{,t} + \mathbf{v}\cdot\nabla\left(\frac{\nabla\cdot\mathbf{B}}{\varrho}\right) = 0. \tag{16}$$

As the above equation advects the quantity $\nabla\cdot\mathbf{B}/\varrho$ we infer that a new *divergence wave* propagates with the speed $\mathbf{v}$. As a result, a partially conservative form of the multi-dimensional equations, obtained by adding terms proportional to $\nabla\cdot\mathbf{B}$, adds an eighth wave that advects $\nabla\cdot\mathbf{B}$ as a passive scalar.

The original MHD equations can be written in the quasi-linear form

$$\overline{\mathbf{q}}_{,t} + \mathbf{A}\overline{\mathbf{q}}_{,x} = 0 \tag{17}$$

with

$$\overline{\mathbf{q}} = (\varrho, \varrho\mathbf{v}, \mathbf{B}, p)^T, \tag{18}$$

$$\mathbf{A} = \begin{pmatrix} v_x & \varrho & 0 & 0 & 0 & 0 & 0 & 0 \\ 0 & v_x & 0 & 0 & -\frac{B_x}{\varrho} & \frac{B_y}{\varrho} & \frac{B_z}{\varrho} & \frac{1}{\varrho} \\ 0 & 0 & v_x & 0 & -\frac{B_y}{\varrho} & -\frac{B_x}{\varrho} & 0 & 0 \\ 0 & 0 & 0 & v_x & -\frac{B_z}{\varrho} & 0 & -\frac{B_x}{\varrho} & 0 \\ 0 & 0 & 0 & 0 & 0 & 0 & 0 & 0 \\ 0 & B_y & -B_x & 0 & -v_y & v_x & 0 & 0 \\ 0 & B_z & 0 & -B_x & -v_z & 0 & v_x & 0 \\ 0 & \gamma p & 0 & 0 & (\gamma-1)\mathbf{v}\cdot\mathbf{B} & 0 & 0 & v_x \end{pmatrix}. \tag{19}$$

Note that a consequence of $(\nabla\cdot\mathbf{B})_{,t} = 0$ the 5-th row from the top of $\mathbf{A}$ contains zeros. As a result of that, we infer that the 8-th eigenvalue of $\mathbf{A}$ is zero, *i. e.*

$$w^8{}_{,t} + 0w^8{}_{,x} = 0 \tag{20}$$

with $w^8 = B_x$.

Equation (14) for $\mathbf{q} = \overline{\mathbf{q}}$ can be rewritten as

$$\overline{\mathbf{q}}_{,t} + \mathbf{A}\overline{\mathbf{q}}_{,x} = -\begin{pmatrix} 0 & 0 & 0 & 0 & 0 & 0 & 0 & 0 \\ 0 & 0 & 0 & 0 & \frac{B_x}{\varrho} & 0 & 0 & 0 \\ 0 & 0 & 0 & 0 & \frac{B_y}{\varrho} & 0 & 0 & 0 \\ 0 & 0 & 0 & 0 & \frac{B_z}{\varrho} & 0 & 0 & 0 \\ 0 & 0 & 0 & 0 & v_x & 0 & 0 & 0 \\ 0 & 0 & 0 & 0 & v_y & 0 & 0 & 0 \\ 0 & 0 & 0 & 0 & v_z & 0 & 0 & 0 \\ 0 & 0 & 0 & 0 & (\gamma-1)\mathbf{v}\cdot\mathbf{B} & 0 & 0 & 0 \end{pmatrix}\overline{\mathbf{q}}_{,x}. \tag{21}$$

Here $\mathbf{A}$ is the matrix defined by Eq. (19). The above equation can be rewritten in the quasilinear form

$$\overline{\mathbf{q}}_{,t} + \overline{\mathbf{A}}\overline{\mathbf{q}}_{,x} = 0 \tag{22}$$

with

$$\overline{\mathbf{A}} = \begin{pmatrix} v_x & \varrho & 0 & 0 & 0 & 0 & 0 & 0 \\ 0 & v_x & 0 & 0 & 0 & \frac{B_y}{\varrho} & \frac{B_z}{\varrho} & \frac{1}{\varrho} \\ 0 & 0 & v_x & 0 & 0 & -\frac{B_x}{\varrho} & 0 & 0 \\ 0 & 0 & 0 & v_x & 0 & 0 & -\frac{B_x}{\varrho} & 0 \\ 0 & 0 & 0 & 0 & v_x & 0 & 0 & 0 \\ 0 & B_y & -B_x & 0 & 0 & v_x & 0 & 0 \\ 0 & B_z & 0 & -B_x & 0 & 0 & v_x & 0 \\ 0 & \gamma p & 0 & 0 & 0 & 0 & 0 & v_x \end{pmatrix}. \tag{23}$$

It is clear that the zero row has disappeared and the eight wave now satisfies the advection equation

$$w^8{}_{,t} + v_x w^8{}_{,x} = 0. \tag{24}$$

As this wave carries non-zero magnetic field divergence it is nicknamed the *divergence* wave.

2.3. Eigenvalues and eigenvectors of the Jacobian matrix. The Jacobian matrix $\overline{\mathbf{A}}$ has the eigenvalues (λ) and left ($\mathbf{l}$) and right ($\mathbf{r}$) eigenvectors which correspond to the following waves [16]:

(a) four magnetoacoustic waves with:

$$\lambda^{\pm} = v_x \pm c_{\pm}, \tag{25}$$

$$\mathbf{l}^{\pm} = N^{\pm} \begin{pmatrix} 0 \\ \pm\varrho c_{\pm} \\ \mp\dfrac{B_x B_y \varrho c_{\pm}}{\varrho c_{\pm}^2 - B_x^2} \\ \mp\dfrac{B_x B_z \varrho c_{\pm}}{\varrho c_{\pm}^2 - B_x^2} \\ 0 \\ \dfrac{B_y \varrho c_{\pm}^2}{\varrho c_{\pm}^2 - B_x^2} \\ \dfrac{B_z \varrho c_{\pm}^2}{\varrho c_{\pm}^2 - B_x^2} \\ 1 \end{pmatrix}^T, \tag{26}$$

$$\mathbf{r}^{\pm} = N^{\pm} \begin{pmatrix} \varrho \\ \pm c_{\pm} \\ \mp\dfrac{B_x B_y c_{\pm}}{\varrho c_{\pm}^2 - B_x^2} \\ \mp\dfrac{B_x B_z c_{\pm}}{\varrho c_{\pm}^2 - B_x^2} \\ 0 \\ \dfrac{B_y \varrho c_{\pm}^2}{\varrho c_{\pm}^2 - B_x^2} \\ \dfrac{B_z \varrho c_{\pm}^2}{\varrho c_{\pm}^2 - B_x^2} \\ \gamma p \end{pmatrix}.$$

Here $N^{\pm}$ stands for a normalization factor such that $\mathbf{l}^{\pm}\mathbf{r}^{\pm} = 1$. This factor is too complicated to be printed here. The superscript $\pm$ corresponds to the fast (c_+) and slow (c_-) magnetoacoustic wave speeds;

(b) two Alfvén waves with:

$$\lambda^a = v_x \pm c_{\mathrm{A}}, \tag{27}$$

$$\mathbf{l}^a = \frac{1}{2\sqrt{N}}\left(0, 0, -B_z, B_y, 0, \pm\frac{B_z}{\sqrt{\varrho}}, \mp\frac{B_y}{\sqrt{\varrho}}, 0\right), \tag{28}$$

$$\mathbf{r}^a = \frac{1}{\sqrt{N}}\left(0, 0, -B_z, B_y, 0, \pm B_z\sqrt{\varrho}, \mp B_y\sqrt{\varrho}, 0\right)^T. \tag{29}$$

Here $N = 1/(B_y^2 + B_z^2)$ is a normalized factor and the Alfvén speed $c_{\mathrm{A}} = B_x/\sqrt{\varrho}$;

(c) one entropy wave with:

$$\lambda^e = v_x, \tag{30}$$

$$\mathbf{l}^e = \left(1, 0, 0, 0, 0, 0, 0, \frac{-1}{c_s^2}\right), \tag{31}$$

$$\mathbf{r}^e = (1, 0, 0, 0, 0, 0, 0, 0)^T. \tag{32}$$

Here the entropy s is defined as

$$s = \log\left(\frac{p}{\varrho^\gamma}\right); \tag{33}$$

(d) one divergence wave with:

$$\lambda^{div} = v_x, \tag{34}$$

$$\mathbf{l}^{div} = (0, 0, 0, 0, 1, 0, 0, 0), \tag{35}$$

$$\mathbf{r}^{div} = (0, 0, 0, 0, 1, 0, 0, 0)^T. \tag{36}$$

The Alfvén eigenvectors become singular when

$$B_\perp \equiv \sqrt{B_y^2 + B_z^2} \to 0. \tag{37}$$

The magnetoacoustic eigenvectors are singular for $c_\pm^2 \to c_{\mathrm{A}}^2$, $c_+^2 \to c_-^2$. In the latter limit the wave speeds c_-, c_+, and c_{A} coincide. One has to deal with these singularities before editing any code. The first solution to this problem was provided by [12]. Another approach was made by [17]. We describe it in some details in the text below.

Let us define

$$\beta_y = \frac{B_y}{B_\perp}, \qquad \beta_z = \frac{B_z}{B_\perp}. \tag{38}$$

Then, the Alfvén eigenvectors can be written as follows:

$$\mathbf{l}^{a\pm} = \frac{1}{2}\Big(0, 0, \pm\beta_z, \mp\beta_y, 0, -\frac{\beta_z \mathrm{sgn}(B_x)}{\sqrt{\varrho}}, \frac{\beta_y \mathrm{sgn}(B_x)}{\sqrt{\varrho}}, 0\Big), \tag{39}$$

$$\mathbf{r}^{a\pm} = (0, 0, \pm\beta_z, \mp\beta_y, 0, -\beta_z\sqrt{\varrho}\mathrm{sgn}(B_x), \beta_y\sqrt{\varrho}\mathrm{sgn}(B_x), 0)^T. \tag{40}$$

The singularities in the Alfvén speed can be fixed by implying [12]

$$\lim_{B_\perp \to 0} \beta_y = \lim_{B_\perp \to 0} \beta_z = \frac{1}{\sqrt{2}}. \tag{41}$$

An elegant way of implementing the above limit into a code is to set

$$\beta_y = \frac{B_y + \epsilon}{B_\perp + \epsilon\sqrt{2}}, \qquad \epsilon \ll 1. \tag{42}$$

Now, we define

$$\alpha_-^2 = \frac{c_s^2 - c_-^2}{c_+^2 - c_-^2}, \qquad \alpha_+^2 = \frac{c_+^2 - c_s^2}{c_+^2 - c_-^2}. \tag{43}$$

A lengthy algebra leads to the eigenvectors for the magnetoacoustic waves [18]

$$\mathbf{l}^+ = \frac{1}{2c_s^2}\begin{pmatrix} 0 \\ \pm\alpha_+ c_+ \\ \mp\alpha_- c_- \beta_y \,\mathrm{sgn}(B_x) \\ \mp\alpha_- c_- \beta_z \,\mathrm{sgn}(B_x) \\ 0 \\ \alpha_- c_s \beta_y/\sqrt{\varrho} \\ \alpha_- c_s \beta_z/\sqrt{\varrho} \\ \alpha_+/\varrho \end{pmatrix}^T,$$

$$\mathbf{r}^+ = \begin{pmatrix} \alpha_+ \varrho \\ \pm\alpha_+ c_+ \\ \mp\alpha_- c_- \beta_y \,\mathrm{sgn}(B_x) \\ \mp\alpha_- c_- \beta_z \,\mathrm{sgn}(B_x) \\ 0 \\ \alpha_- c_s \beta_y \sqrt{\varrho} \\ \alpha_- c_s \beta_z \sqrt{\varrho} \\ \alpha_+ \varrho c_s^2 \end{pmatrix}, \tag{44}$$

$$\mathbf{l}^- = \frac{1}{2c_s^2}\begin{pmatrix} 0 \\ \pm\alpha_- c_- \\ \pm\alpha_+ c_+ \beta_y \,\mathrm{sgn}(B_x) \\ \pm\alpha_+ c_+ \beta_z \,\mathrm{sgn}(B_x) \\ 0 \\ -\alpha_+ c_s \beta_y/\sqrt{\varrho} \\ -\alpha_+ c_s \beta_z/\sqrt{\varrho} \\ \alpha_-/\varrho \end{pmatrix}^T,$$

$$\mathbf{r}^- = \begin{pmatrix} \alpha_- \varrho \\ \pm\alpha_- c_- \\ \pm\alpha_+ c_+ \beta_y \,\mathrm{sgn}(B_x) \\ \pm\alpha_+ c_+ \beta_z \,\mathrm{sgn}(B_x) \\ 0 \\ -\alpha_+ c_s \beta_y \sqrt{\varrho} \\ -\alpha_+ c_s \beta_z \sqrt{\varrho} \\ \alpha_- \varrho c_s^2 \end{pmatrix}. \tag{45}$$

These eigenvectors contain only the triple umbilic singularity which occurs at $c_+^2 = c_-^2 = c_\mathrm{A}^2$ when $B_\perp \to 0$. The triple umbilic point occurs, where the fast, slow, and Alfvén speeds coincide. It can be shown that around this point

$$\alpha_- = \cos\frac{\alpha}{2} + \delta_-, \qquad \alpha_+ = \sin\frac{\alpha}{2} + \delta_+ \tag{46}$$

with

$$\tan\alpha \equiv \frac{B_x - c_s\sqrt{\varrho}}{B_\perp}. \tag{47}$$

The errors $\delta_\pm$ satisfy

$$|\delta_\pm| \le \frac{B_\perp}{4c_s\sqrt{\varrho}}. \tag{48}$$

For $B_\perp = 0$ it can be proved that $\alpha_- = H(B_x - c_s\sqrt{\varrho})$ and $\alpha_+ = H(c_s\sqrt{\varrho} - B_x)$, where H is the Heaviside function [18].

3. Difficulties with numerical solutions of the MHD equations

An important problem in developing a scheme for the MHD equations is that these equations are neither strictly hyperbolic nor strictly convex [12]. The MHD equations form a non-strictly hyperbolic system as some eigenvalues may coincide at some points and that compound wave structures, involving both shocks and rarefactions, may sometimes develop. It occurs that when the magnetic field components disappear the eigenvectors become singular. By renormalizing the eigenvectors, these singularities can be removed [8, 12].

Contrary to the hydrodynamic case, the Riemann problem [1] for the ideal MHD is not completely consistent and unique as one of the eigenvalues of the Jacobian matrix is zero, see Eq. (20). This zero eigenvalue is non-physical as the eigenvalues should appear either singly as the x-component of the flow, v_x, or in pairs symmetric about v_x. Physical eigenvalues and eigenvectors are given by Eqs. (25)–(36).

The zero eigenvalue leads to numerical difficulties associated with nonzero divergence of the magnetic field. Consequently, characteristics can become degenerate, depending on the orientation of the magnetic field. It turns out that the solution of this problem is to consider a form of the equations that is not strictly in a conservation form [16]. See Eq. (14).

3.1. Divergence cleaning methods. There are several important issues in developing a new MHD code. One of these is ensuring $\nabla \cdot \mathbf{B} = 0$ [13, 19, 20]. Clearly, the discretization errors lead to non-zero divergence over time. Physically, this means that nothing maintains conservation of a magnetic flux in the Gauss' law. Several remedies have been proposed. Dedner et al. [21] proposed a method of adding a diffusion term in the induction equation that makes the divergence-free error diffuse away from the source. By this term magnetic monopoles are locally suppressed but they are not completely eliminated [14, 15, 21], among others, utilized a numerical technique called *constraint transport* to transform the induction equation in such a way that it maintains vanishing divergence of the field components to within machine round-off error. This can be done by placing field components at appropriate locations of a numerical cell. This technique was implemented in a number of numerical codes (e.g., [4, 13–15, 22, 23]).

Here we list few traditional approaches to enforce the divergence-free constraint:

(a) a direct magnetic flux function, $\mathbf{B} = \nabla \times \mathbf{A}$, approach. Obviously, the divergence-free condition is satisfied automatically. The difficulty with this approach is that a representation of the Lorentz force requires taking a second derivative of the flux function, $\mathbf{A}$. That forces an application of the higher-order numerical schemes. Even then, one can encounter serious problems due to anomalous Lorentz force which apparently reveals itself in the neighborhood of large spatial gradients;

(b) a projection scheme which forces the divergence-free constraint by solving a Poisson equation to subtract off the portion of the magnetic field that leads to non-zero divergence [24]. Suppose that magnetic field has a non-zero divergence, $\nabla \cdot \mathbf{B} \neq 0$. We can fix this problem by adding a correction term $\mathbf{B}_c$ such that

$$\nabla \cdot (\mathbf{B} + \mathbf{B}_c) = 0. \tag{49}$$

Clearly, to have the Lorentz force zero $\mathbf{B}_c$ must not generate new current $\mathbf{j}_c = \dfrac{1}{\mu}(\nabla \times \mathbf{B}_c) = \mathbf{0}$. Hence,

$$\nabla \times \mathbf{B}_c = 0, \tag{50}$$

from which we infer that

$$\mathbf{B}_c = \nabla \phi. \tag{51}$$

Here ϕ is a scalar potential. Substituting Eq. (51) into Eq. (49) we obtain

$$\nabla^2 \phi = -\nabla \cdot \mathbf{B}. \tag{52}$$

This is the Poisson equation which has to be solved in the whole computational domain. The resulting solution ϕ should be used to evaluate $\mathbf{B}_c$ according to Eq. (51) and this to clean the magnetic field $\mathbf{B}$. However, this method has its disadvantages. Its major drawback is that it requires a global solution to the elliptic Eq. (52) which is computationally expensive. Moreover, the global nature of the cleaning procedure violates the hyperbolicity of the MHD equations in regions where the flow is supersonic and superalfvénic [25];

(c) a staggered-grid approach in which the divergence-free constraint is satisfied by placing the magnetic field components at the centroids of appropriate cell faces and remnant plasma variables such as mass, momentum and energy are stored at the centroids of computational cells. On such a grid the MHD equations can be approximated in a way that preserves selenoidality of discrete magnetic field [4, 14, 15, 22, 23]. This approach comes from incompressible fluid mechanics where the velocity field must be kept divergence-free. However, staggered grids are expensive for storage and handling on meshes with hanging nodes that are common to unstructured grid methods;

(d) the truncation-level error method which was developed by Powell [16] and used by [26, 27], and [28]. This approach relies on an addition to the original set of the MHD equations the source term that is proportional to $\nabla \cdot \mathbf{B}$. See Eq. (14). By that way any local $\nabla \cdot \mathbf{B}$ that is created is convected away in accordance to Eq. (16). It was found by Janhunen [29] that in the case when the contribution to the total energy from the fluid pressure is small in comparison to the magnetic and kinetic energies this approach may lead to an unphysical intermediate state with negative fluid pressure. As a consequence of that computing the pressure from the conserved quantities may involve the difference between two nearly equal terms and the numerical errors result. Janhunen [29] showed that this problem can be overcome by discarding the source terms in the energy and momentum equations, so that Eq. (14) becomes

$$\mathbf{q}_{,t} + \nabla \cdot \mathbf{F} = -\nabla \cdot \mathbf{B}(0, 0, \mathbf{v}, 0)^T, \qquad \nabla \cdot \mathbf{B} = 0; \tag{53}$$

(e) a parabolic divergence cleaning method which is based on a modified system in which the divergence constraint is coupled with the conservation laws by introducing a generalized Lagrange multiplier. Such formulation results in the divergence errors transported to the domain boundaries with the maximal admissible speed while they are damped simultaneously. See [23] for details;

(e) the unstaggered constraint transport method was developed by [13]. In this method all quantities, including all components of the magnetic field and magnetic flux function which expresses the magnetic field, are treated as cell-centered. A high-resolution wave propagation scheme for evolving the magnetic flux function was developed. In a recent extension of the method to a 3D case this scheme results in the transport equation that must be solved for the magnetic flux function is only weakly hyperbolic and the problem of weak hyperbolicity was handled [20].

4. Numerical results

As a consequence of complexity of MHD waves in highly inhomogeneous plasma it is necessary to understand simpler phenomena which may play the role of elementary building blocks in the construction of a more elaborated theory. As a result, our strategy is to develop simpler models at the initial stage of the research and progressively extend and generalize them to more complex models at subsequent stages. Therefore in this study, we assume that at the equilibrium the solar atmosphere is settled in a two-dimensional (2D) and still ($\mathbf{V} = \mathbf{0}$) environment. At the equilibrium, the pressure gradient force is balanced by the gravity, that is

$$-\nabla p + \varrho \mathbf{g} = 0. \tag{54}$$

Here we set $g = 2.74 \cdot 10^2$ m s^{-2}. Using the equation of state, given in Eq. (6), and the y-component of hydrostatic pressure balance indicated by Eq. (54), we obtain equilibrium gas pressure and mass density as

$$p(y) = p_0 \ \exp\left(-\int_{y_r}^{y} \frac{dy'}{\Lambda(y')}\right), \tag{55}$$

$$\varrho(y) = \frac{p(y)}{g\Lambda(y)}. \tag{56}$$

Here

$$\Lambda(y) = k_{\mathrm{B}} T(y)/(mg) \tag{57}$$

is the pressure scale-height, and p_0 denotes the gas pressure at the reference level, $y = y_r$, which we choose and set fixed as $y_r = 10$ Mm.

We adopt a realistic temperature profile $T(y)$ for the solar atmosphere [30], which is displayed in Fig. 1. Note that T attains a value of about 5700 K at the top of the photosphere which corresponds to $y = 0.5$ Mm. At higher altitudes $T(y)$ falls off until it reaches its minimum of 4350 K at the altitude of $y \simeq 0.95$ Mm. Higher up $T(y)$ grows gradually with height up to the transition region which is located at $y \simeq 2.7$ Mm. Here $T(y)$ experiences a sudden growth up to the coronal value of 1.5 MK at $y = 10$ Mm. Having specified $T(y)$ with a use of Eqs. (55) and (60) we can obtain mass density and gas pressure profiles.

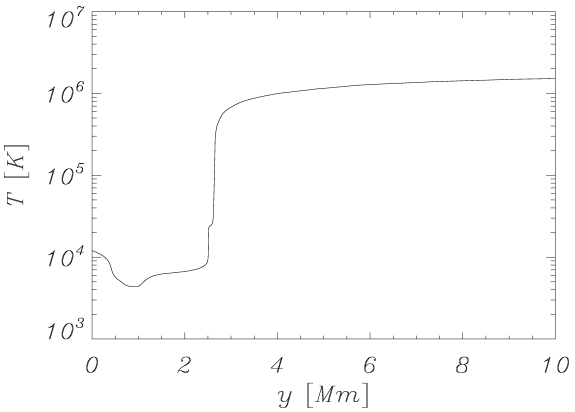

Fig. 1. Equilibrium temperature (in Kelvins) profile vs. height y (in Mm) for the solar atmosphere

For the initial magnetic field, we adopt the model which was devised by Priest [31]. In this model, we assume that magnetic field is current-free ($\nabla \times \mathbf{B} = \mathbf{0}$) and potential ($\mathbf{B} = \nabla \times (A\hat{\mathbf{z}})$) with the magnetic flux function

$$A(x, y) = B_0 \Lambda_B \cos(x/\Lambda_B) \exp[-(y - y_r)/\Lambda_B]\,. \qquad (58)$$

Here B_0 denotes the magnetic field at $y = y_r$ and $\Lambda_B = 2L/\pi$ is the magnetic scale-height. We choose $2L = 30$ Mm which correspond to the size of a supergranular cell. It is noteworthy that the magnetic field is predominantly vertical at supergranular boundaries ($x = 0$, $x = 2L$), while it reveals a horizontal canopy structure at the supergranular center ($x = L$).

A magnitude of magnetic field is chosen to specify at $y = y_r$ the plasma $\beta = 2\mu p/B^2 = 2c_s^2/(\gamma c_A^2)$ equal to 0.048. Here the sound speed $c_s = \sqrt{\gamma p/\varrho}$ and the Alfvén speed, $c_A = \sqrt{B^2/(\mu\varrho)}$. Figure 2 illustrates vertical profile of the plasma β which attains a value of about 0.015 around the transition region, $y \simeq 2.7$ Mm, while it grows with depth reaching a value of about 6 at $y = 1.5$ Mm that is located within the solar chromosphere. This growth results from the abrupt increase of gas pressure there.

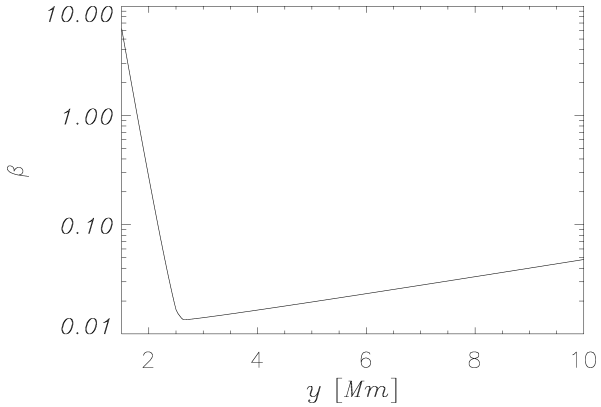

Fig. 2. The plasma β profile vs. height y

We excite waves in the above described solar atmosphere by launching initially, at $t = 0$, the Gaussian pulse in a vertical component of velocity V_y, i.e.

$$V_y(x, y, t = 0) = A_v \exp\left[-\frac{x^2 + (y - y_0)^2}{w^2}\right]. \qquad (59)$$

Here $A_v = 5$ km s^{-1} is the amplitude of the pulse, $y_0 = 0.5$ Mm is its vertical position and $w = 0.3$ Mm is its width.

Equations (1)–(6) are solved numerically using the code FLASH [27] which implements a second-order unsplit Godunov solver and Adaptive Mesh Refinement (AMR). We set the simulation box as $(-15, 15)$ Mm $\times(-0.5, 29.5)$ Mm and fix at all four boundaries of the simulation region the plasma quantities to their equilibrium values. In our studies we use AMR grid with a minimum (maximum) level of refinement blocks set to 5 (8). The refinement strategy is based on controlling numerical errors in a gradient of mass density. Such settings result in an excellent resolution of steep spatial profiles, which significantly reduce numerical diffusion within the simulation region.

Figure 3 illustrates spatial profiles of $\log\varrho$ and velocity vectors at $t = 250$ s (left panel) and $t = 1500$ s (right panel). The initial pulse splits in a usual way into counter-propagating waves. The wave propagating upwards grows in its amplitude as a result of the rapid decrease of mass density in the chromosphere. As a consequence of that a shock results in. Photospheric and chromospheric plasma is lifted up by underpressure which settles in below the shock. The pressure gradient force overwhelms gravity and it pushes the photospheric and chromospheric material towards the solar corona. This scenario is clearly seen at $t = 250$ s. At a later time the plasma becomes attracted by gravity and as a result is falls off towards the low layers. However, the secondary shock which results from the original pulse works against this fall off as it lifts up the photospheric and chromospheric plasma. As a result, a complex bi-directional flows arises. The whole scenario bares many features of solar spicules. It is noteworthy that the magnetic field-free case, $\mathbf{B} = \mathbf{0}$, was recently discussed by Gruszecki et al. [32] who revealed similar features of quasi-periodic shocks traveling from the chromosphere to the corona. However, in this hydrodynamic case spatial wave profiles were more symmetric in space and spicules were not observed.

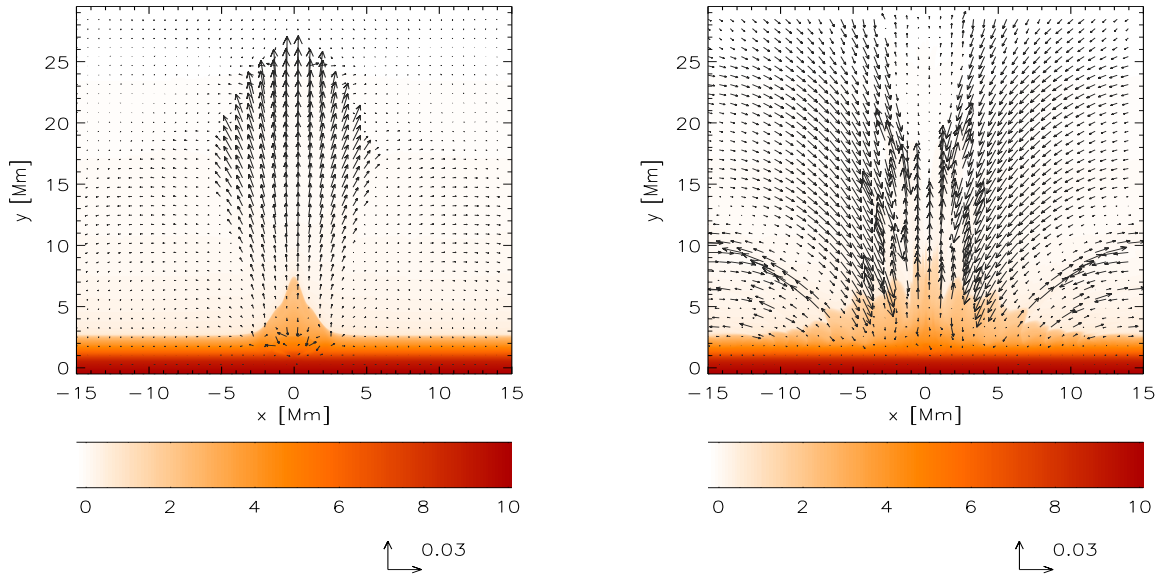

Fig. 3. Mass density (colour maps, log scale) and velocity (arrows) profiles at $t = 250$ s (left panel) and $t = 1500$ s (right panel). Mass density and velocity are expressed in units of 10^{-12} kg m^{-3} and 1 Mm s^{-1}, respectively

Figure 4 displays time-signatures of the vertical component of velocity for the case of Fig. 3. This velocity is collected in time at the detection point ($x = 0$, $y = 20$) Mm. The arrival of the shock front to the detection point occurs at $t \simeq 200$ s. The second, third, and fourth shocks fronts reach the detection point at $t \simeq 350$ s, $t \simeq 650$ s, and $t \simeq 950$ s, respectively. This secondary shock results from the nonlinear wake which lags behind the leading signal. In the linear approximation and magnetic-free case, the wake oscillates with the acoustic cut-off frequency

$$\Omega_{\rm ac} = \frac{c_{\rm s}}{2\Lambda}\sqrt{1 + 2\frac{d\Lambda}{dy}}. \tag{60}$$

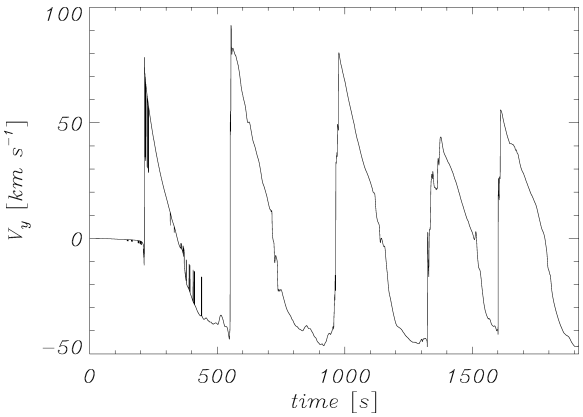

Fig. 4. The plasma β profile vs. height y

This scenario consists the building block of one-dimensional (1D) rebound shock model of [33] who proposed that the secondary shock (or rebound shock) lifts up the transition region higher than the first shock thereby resulting in a spicule appearance at observed heights. The process is well studied in the frame of 1D numerical simulations. However, our 2D numerical simulations introduce new interesting features in comparison to the 1D rebound shock scenario.

There are few conclusions which result from our simulations:

a) according to the theory of Klein-Gordon equation an initial pulse generates a wave front and a trailing wake which oscillates with acoustic cut-off frequency [33];
b) even a small amplitude initial pulse launched at the top of the photosphere exhibits a tendency to generate shocks. These shocks result from a nonlinear wake.

5. Summary

This paper presents several mathematical aspects in numerical methods for magnetohydrodynamic equations. Although this presentation is far from complete the emphasis is on the methods which are the most effective and the best known to the author.

There are several conditions that numerical schemes should satisfy: accuracy and speed of numerical simulations, adequate representation of complex flows and steep profiles, lack of generation of spurious oscillations as well as *robustness*. A computer code is called robust if it has the virtue of giving reliable results to a wide range of problems without needing to be retuned. Numerical schemes such as shock-capturing schemes described in this paper satisfy these conditions.

Existing numerical models such as was used in Sec. 4 with an adaptation of the FLASH code demonstrate the feasibility of fluid simulations in obtaining at least qualitative and, to some extent, quantitative features in the magnetized fluid. With continued improvements in computational methods and computer resources, the usefulness and capability of the numerical approach should continue to improve.

Acknowledgements. The software used in this work was in part developed by the DOE-supported ASCI/Alliance Center for Astrophysical Thermonuclear Flashes at the University of Chicago.

REFERENCES

[1] E. Toro, *Riemann Solvers and Numerical Methods for Fluid Dynamics*, Springer, Berlin, 2009.
[2] R.J. LeVeque, *Finite-volume Methods for Hyperbolic Problems*, Cambridge University Press, Cambridge, 2002.
[3] S.K. Godunov, "A difference scheme for numerical solution of discontinuos solution of hydrodynamic equations", *Math. Sb.* 47, 271–306 (1959).
[4] J.M. Stone and M.L. Norman, "ZEUS-2D: a radiation magnetohydrodynamics code for astrophysical flows in two space dimensions. II. The magnetohydrodynamic algorithms and tests", *Astrophys. J. Suppl. Ser.* 80, 791–818 (1992).
[5] K. Murawski and R.S. Steinolfson, "Numerical modeling of the solar wind interaction with Venus", *Planet. Space Sci.* 44, 243–252 (1996).
[6] K. Murawski and D. Lee, "Numerical methods of solving equations of hydrodynamics from perspectives of the code FLASH", *Bull. Pol. Ac.: Tech.* 59 (1), 81–91 (2011).
[7] P.R. Woodward and P. Colella, "The numerical simulation of two-dimensional fluid flow with strong shocks", *J. Comp. Phys.* 54, 115–173 (1984).
[8] P.L. Roe and D.S. Balsara, "Notes on the eigensystem of magnetohydrodynamics", *SIAM J. Appl. Math.* 56, 57–67 (1996).
[9] A.A. Barmin, A.G. Kulikovskiy, and N.V. Pogorelov, "Shock-capturing approach and nonevolutionary solutions in magnetohydrodynamics", *J. Comp. Phys.* 126, 77–90 (1996).
[10] J.U. Brackbill and D.C. Barnes, "The effect of nonzero $\nabla \cdot \mathbf{B}$ on the numerical solution of the magnetohydrodynamic equations", *J. Comp. Phys.* 35, 426 (1980).
[11] K. Murawski, *Analytical and Numerical Methods for Wave Propagation in Fluids*, World Scientific, Singapore, 2002.
[12] M. Brio and C.C. Wu, "An upwind differencing scheme for the equations of ideal magnetohydrodynamics", *J. Comp. Phys.* 75, 400–422 (1988).
[13] J.A. Rossmanith, "An unstaggered, high-resolution constrained transport method for magnetohydrodynamic flows", *SIAM J. Sci. Comp.* 28, 1766–1797 (2006).
[14] U. Ziegler, "The NIRVANA code: Parallel computational MHD with adaptive mesh refinement", *Computer Phys. Comm.* 179, 227–244 (2008).
[15] J.M. Stone, T.A. Gardiner, P. Teuben, J.F. Hawley, and J.B. Simon, "Athena: a new code for astrophysical MHD", *Astrophysical J. Supplement Series* 178, 137–177 (2008).
[16] K.G. Powell, "An approximate Riemann solver for magnetohydrodynamics", *ICASE Report* 94–24, CD-ROM (1994).
[17] A.L. Zachary and P. Colella, "A higher-order Godunov method for the equations of ideal magnetohydrodynamics", *J. Comp. Phys.* 99, 341–347 (1992).
[18] D.V. Abeele, "Development of a Godunov-type solver for 2D ideal MHD problems", *Project Rep.* 1, CD-ROM 1995.
[19] P.J. Dellar, "A note on magnetic monopoles and the one dimensional MHD Riemann problem", *J. Comp. Phys.* 172, 392–398 (2001).
[20] Ch. Helzel, J.A. Rossmanith, and B. Taetz, "An unstaggered constrained transport method for the 3D ideal magnetohydrodynamic equations", eprint arXiv:1007.2606, (2010).
[21] A. Dedner, F. Kemm, D. Kröner, C.-D. Munz, T. Schnitzer, and M. Wesenberg, "Hyperbolic divergence cleaning for the MHD equations", *J. Comp. Phys.* 175, 645–673 (2002).
[22] C.R. DeVore, "Flux-corrected transport techniques for multidimensional compressible magnetohydrodynamics", *J. Comp. Phys.* 92, 142–160 (1991).
[23] D. Lee and A.E. Deane, "An unsplit staggered mesh scheme for multidimensional magnetohydrodynamics", *J. Comp. Phys.* 228 (4), 952–975 (2009).
[24] T. Tanaka, "Configurations of the solar wind flow and magnetic field around the planets with no magnetic field: calculation by a new MHD simulation scheme", *J. Geophys. Res.* 98, 17251–17262 (1993).
[25] G. Tóth, "The $\nabla \cdot \mathbf{B} = 0$ constraint in shock-capturing magnetohydrodynamics codes", *J. Comp. Phys.* 161, 605–652 (2000).
[26] T.I. Gombosi, D.L. De Zeeuw, R.M. Häberli, and K.G. Powell, "Axisymmetric modeling of cometary mass loading on an adaptively refined grid: MHD results", *J. Geophys. Res.* 99 (21), 525–521, 539 (1994).
[27] N. Aslan, "MHD-A: A fluctuation splitting wave model for planar magnetohydrodynamics", *J. Comp. Phys.* 153, 437–466 (1999).
[28] K.G. Powell, P.L. Roe, T.J. Linde, T.I. Gombosi, and D.L. De Zeeuw, "A solution-adaptive upwind scheme for ideal magnetohydrodynamics", *J. Comp. Phys.* 154, 284–309 (1999).
[29] P. Janhunen, "A positive conservative method for magnetohydrodynamics based on HLL and Roe methods", *J. Comp. Phys.* 160, 649–661 (2000).
[30] J.E. Vernazza, E.H. Avrett, and R. Loeser, "Structure of the solar chromosphere. III – models of the EUV brightness components of the quiet-sun", *Astrophysical J.* 45, 635–725 (1981).
[31] E.R. Priest, *Solar Magnetohydrodynamics*, Reidel Publishing Company, Dordrecht, 1982.
[32] M. Gruszecki, K. Murawski, A.G. Kosovichev, K.V. Parchevsky, and T. Zaqarashvili, "Numerical simulations of impulsively excited acoustic-gravity waves in a stellar atmosphere", *Acta Phys. Polonica*, (2011), (to be published).
[33] J.V. Hollweg, "On the origin of solar spicules", *Astrophys. J.* 257, 345–353 (1982).